# Intrinsic triferroicity in a two-dimensional lattice

Shiying Shen,[1] Xilong Xu,[1] Baibiao Huang,[1] Liangzhi Kou,[2] Ying Dai,[1,*] and Yandong Ma[1,†]
[1]*School of Physics, State Key Laboratory of Crystal Materials, Shandong University, Shandanan Street 27, Jinan 250100, China*
[2]*School of Chemistry, Physics and Mechanical Engineering, Queensland University of Technology, Brisbane, Queensland, 4001, Australia*

(Received 11 May 2020; accepted 29 March 2021; published 8 April 2021)

Intrinsic triferroicity is essential and highly sought for novel device applications, such as high-density multistate data storage. So far, the intrinsic triferroicity has only been discussed in three-dimensional systems. Herein on the basis of first principles, we report the intrinsic triferroicity in a two-dimensional lattice. Being exfoliatable from the layered bulk, single-layer $FeO_2H$ is shown to be an intrinsically triferroic semiconductor, presenting antiferromagnetism, ferroelasticity, and ferroelectricity simultaneously. Moreover, the directional control of its ferroelectric polarization is achievable by 90° reversible ferroelastic switching. In addition, single-layer $FeO_2H$ is identified to harbor in-plane piezoelectric effect. The unveiled phenomena and mechanism of triferroics in this two-dimensional system not only broaden the scientific and technological impact of triferroics but also enable a wide range of nanodevice applications.

DOI: 10.1103/PhysRevB.103.144101

## I. INTRODUCTION

Ferroics is essential to many forms of current and next-generation information technology by virtue of the polarization-switching properties [1–3]. It mainly includes ferromagnets, ferroelectrics, and ferroelastics. In each case, crystal symmetry is broken by the coalignment of a particular type of internal degree of freedom, that is, spin orientation for ferromagnets, dipolar displacement for ferroelectrics, and structure deformation for ferroelastics. When two or three ferroic orders coexist in a single-phase material, the multiferroics is achieved [4–11], allowing for a variety of appealing phenomena; for example, the magnetization of a system might be inverted by applying an electric field [9–11]. Beyond ferroic orders, the multiferroics has been broadened to include antiferroic orders, such as antiferromagnets and antiferroelectrics [4–8]. Among different types of multiferroics, undoubtedly, intrinsic triferroics that holds simultaneously three (anti)ferroic orders is most desirable as it possesses unprecedented opportunities for intriguing physics; its exploitation promises multifunctional and controllable device applications [4–11].

To date, the concept of intrinsic triferroics has only been discussed in three-dimensional (3D) systems [4,5,12]. It is fascinating to note that many fundamental physical phenomena in 3D materials and devices have always found their way to two-dimensional (2D) counterparts, such as superconductors [12,13], topological insulators [14–16], and field-effect transistors [17,18]. In general, 2D counterparts have the added advantages of high storage density, low energy consumption, fast device operation, and mechanical flexibility. These, combined with technological aspiration of miniaturizing devices, make the achievement of 2D counterparts a highly sought-after target. Actually, many experimental and theoretical studies on 2D ferroics have been reported in the literature [19–26], and even a few on 2D intrinsic multiferroics that entail two (anti)ferroic orders simultaneously [27–32]. Therefore, an interesting question is whether intrinsic triferroics can be realized in a 2D lattice.

In this work, we demonstrate that intrinsic triferroics can indeed be realized in a 2D lattice. Based on first-principles calculations, we show that single-layer (SL) $FeO_2H$ is an intrinsically triferroic semiconductor, harboring antiferromagnetism, ferroelasticity, and ferroelectricity simultaneously. The physical origin of triferroics has been explained based on the structure and atomic arrangement. This 2D crystal has great thermal and dynamical stabilities as well as easy experimental fabrication from its layered bulk. Furthermore, we predict that such a system could demonstrate many distinctive properties, for example, the directional control of ferroelectric polarization by ferroelastic switching and the in-plane piezoelectric effect. These findings will be useful for fundamental research in triferroics and promote technological innovation in nanodevices.

## II. RESULTS

Magnetism originates from a transition-metal atom with partially filled $d$ shells, because the spins of the electrons occupying fully filled shells add to zero and do not participate in magnetics. To realize the partially filled $d$ shells, the local structure symmetry, namely, coordinated environment, is an essential ingredient. Thus, the combination of transition-metal atom and proper coordinated environment is responsible for the appearance of magnetism. SL $FeO_2H$ is one promising candidate due to the presence of a partially filled $d$ shell of iron. Figure 1 displays the crystal structure of SL $FeO_2H$ belonging to space group $Pmn2_1$ ($C_{2v}$). The

*daiy60@sina.com
†yandong.ma@sdu.edu.cn

 

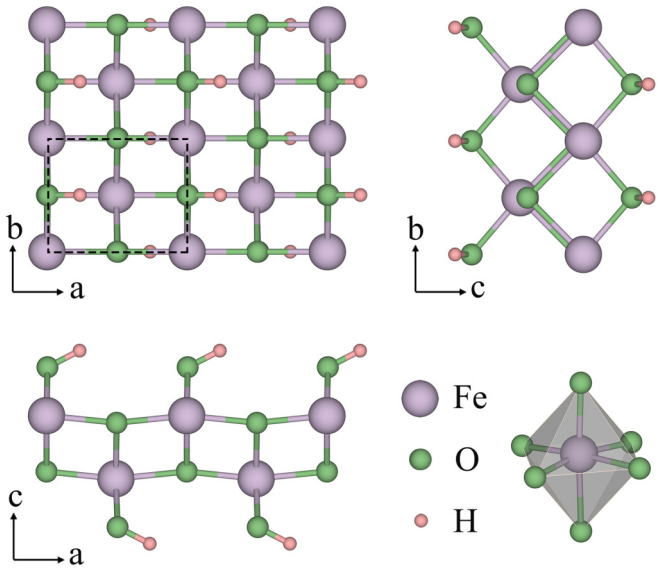


FIG. 1. Crystal structure of SL $FeO_2H$ from top and side views, with the black square marking the primitive cell. Inset shows the distorted $FeO_6$ octahedra.

lattice constants are found to be $a = 3.79$ Å and $b = 3.07$ Å, with one unit cell containing eight atoms, i.e., two Fe in the Wyckoff 2*a* position, four O in the 2*a* position, and two H in the 2*a* position. Each Fe atom is coordinated with four oxygen ($O^{2-}$) and two hydroxide ions ($[OH]^-$), forming a distorted octahedral geometry for the Fe atom as well as the stoichiometric formula of $[Fe^{3+}][O]^{2-}[OH]^-$. Given that the valence electronic configuration of an isolated Fe atom is $3d^6 4s^2$, the half-filled high-spin state (A_1 ↑↑, A_2 ↑, B_1 ↑, and B_2 ↑) is achieved for SL $FeO_2H$, which would give rise to a formal magnetic moment of $5\,\mu_B$ on each Fe atom. Our first-principles calculations show that the magnetic moment on each Fe atom is $4.37\,\mu_B$. This value is a little smaller than $5\,\mu_B$ due to the strong hybridization with O 2*p* orbitals. This indicates a large spin polarization in SL $FeO_2H$. We also calculate the low-spin state of SL $FeO_2H$, which is found to be higher in energy than the high-spin ground state by about 0.60 eV/per atom.

To probe the preferred magnetic order of SL $FeO_2H$, we consider four configurations, including three antiferromagnetic (AFM) state and one ferromagnetic (FM) state; see Fig. S1 in the Supplemental Material [33]. The ground state is found to be AFM-1 shown in Fig. S1 [33], which is lower than the AFM-2, AFM-3, and FM states by 0.11, 0.13, and 0.10 eV/atom, respectively. We also investigate the magnetic ground state of SL $FeO_2H$ by using the Perdew-Burke-Ernzerhof (PBE) functional, and find that AFM-1 remains the ground state, which is lower than that of the AFM-2, AFM-3, and FM states by 0.09, 0.04, and 0.06 eV/atom, respectively. Figure 2(a) shows the band structure of SL $FeO_2H$. Obviously, SL $FeO_2H$ is an AFM semiconductor with an indirect band gap of 2.56 eV. Also, we can see that its conduction band minimum (CBM) is dominated by Fe 3*d* orbitals, while its valence band maximum (VBM) is mainly derived from O 2*p* orbitals. We then study the magnetic anisotropy energy (MAE) of SL $FeO_2H$. The MAE is defined as the difference in energy between the system with a given spin orientation, i.e., $\Delta E = |E_{\rightarrow} - E_{\uparrow}|$, where $E_{\rightarrow}(E_{\uparrow})$ indicates the total energy for in-plane (out of plane) magnetic configuration. This method to estimate MAE is employed in previous works on 2D AFM materials [34,35]. MAE are composed of two parts: the magnetocrystalline anisotropy energy (C MAE) arising from the effect of SOC, and the magnetic dipolar anisotropy energy (D MAE) arising from the dipole-dipole interaction [36,37]. The calculated C-MAE are listed in Table S2 [33], wherein $E_{100}$, $E_{010}$, and $E_{001}$ correspond to the energies with

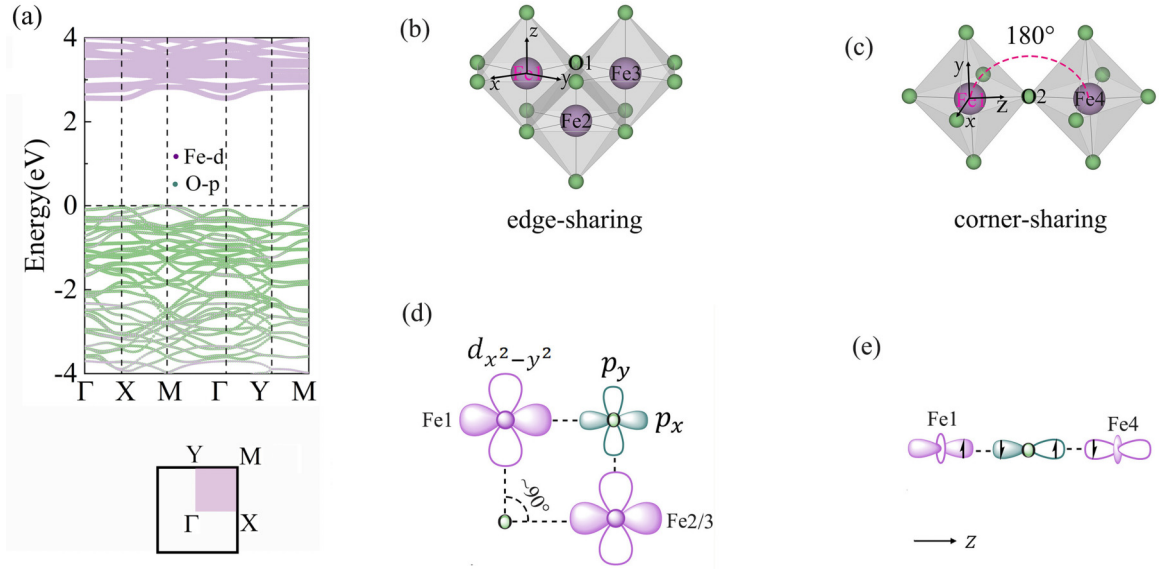


FIG. 2. Magnetism of SL $FeO_2H$. (a) Fat band structure of $FeO_2H$ based on HSE06 functional. The Fermi level is shifted to VBM. Inset in (a) is the first Brillouin zone (BZ) with the high-symmetry points marked. (b) Edge-sharing configuration for adjacent octahedrons. (c) Corner-sharing configuration for adjacent octahedrons. (d) Schematic diagram of the exchange interaction between Fe1 and Fe2/Fe3 in SL $FeO_2H$. (e) Schematic diagram of exchange interaction between Fe1 and Fe4 in SL $FeO_2H$.

the magnetization axes along the (100), (010), and (001) directions. Clearly, the magnetization easy axis is along the $y$ direction (in plane), which is lower in energy than that along the $x$ and $z$ directions by 168 and 267 $\mu$eV per unit cell, respectively. Figure S2 illustrates the C MAE as a function of polar angles in the $yz$ and $xy$ planes [33]. It can be observed that the energies in the $yz$ and $xy$ planes strongly depend on the direction of the magnetization, and the spins in SL $FeO_2H$ are favorably aligned along the $y$ direction. Note that the D MAE always prefers an in-plane magnetization [38]. These facts imply that SL $FeO_2H$ belongs to the category of *XY* magnets. In 2D *XY* magnets, such anisotropic in-plane magnetization can break the restriction of Mermin-Wagner theorem and ensure the (quasi-) long-range ordered phases [39].

The underlying physics of such AFM coupling in SL $FeO_2H$ is related to the competition between the direct- and superexchange interactions. As illustrated in Figs. 2(b) and 2(c), there are two typical connecting configurations for adjacent octahedrons, i.e., edge sharing and corner sharing. In the edge-sharing case, the Fe-O-Fe bond angles are found to be 90 ° roughly [Fig. 2(b)]. According to the well-known Goodenough-Kanamori-Anderson (GKA) rules [40,41], superexchange should dominate the interaction between Fe atoms in SL $FeO_2H$, thus leading to FM coupling between nearest neighboring (NN) Fe atoms (namely, Fe1-Fe2, 2.98 Å) and between next-nearest neighboring (NNN) Fe atoms (namely, Fe1-Fe3, 3.07 Å); see Fig. 2(d). Different from the edge-sharing configuration, in corner-sharing configuration, the Fe1-O-Fe4 bond angle is 180 ° roughly [Fig. 2(c)]. Accordingly, the coupling between next-next nearest neighboring (NNNN) Fe atoms (namely, Fe1-Fe4, 3.79 Å) is AFM; see Fig. 2(e).

Based on the 2D *XY* model, the spin Hamiltonian [39] of single-layer $FeO_2H$ can be considered as

$$H=-J_1\sum_{\langle i,j\rangle}S_iS_j-J_2\sum_{\langle\langle i,j\rangle\rangle}S_iS_j-J_3\sum_{\langle\langle\langle i,j\rangle\rangle\rangle}S_iS_j+D\sum_i\left(S_i^y\right)^2,$$

where $\langle i,j\rangle$, $\langle\langle i,j\rangle\rangle$, and $\langle\langle\langle i,j\rangle\rangle\rangle$ stand for the NN, NNN, and NNNN sites, respectively. Also, $J_1$, $J_2$, and $J_3$ are the NN, NNN, and NNNN spin exchanges, respectively; see Fig. S3 in the Supplemental Material [33]. $S_i^y$ and $D$ are the spin operator and anisotropy energy parameter, respectively. Thus, the total energies of different magnetic configurations (scheme in Fig. S1 [33]) are

$$E_{\rm FM}=E_0-(16J_1+8J_2+8J_3)\times|S|^2+D|S|^2,$$
$$E_{\rm FM}=E_0-(8J_2-8J_3)\times|S|^2+D|S|^2,$$
$$E_{\rm FM}=E_0-(-8J_2+8J_3)\times|S|^2+D|S|^2,$$
$$E_{\rm FM}=E_0-(-16J_1+8J_2+8J_3)\times|S|^2+D|S|^2.$$

Here, $|S|=\frac{5}{2}$, and $E_{\rm FM}$, $E_{\rm AFM1}$, $E_{\rm AFM2}$, $E_{\rm AFM3}$ are the total energy of FM, AFM-1, AFM-2, and AFM-3 configurations, respectively. These total energies of different magnetic configurations are based on identical lattice structure. Combining these equations, we find that $J_1$ is FM (1.399 meV), $J_2$ is FM (0.053 meV), and $J_3$ is AFM (−8.959 meV). The anisotropy energy parameter $D$ is estimated to be −43 $\mu$eV according to $D=(E_{010}-E_{001})/|S|^2$. The phenomena that NNNN exchange interaction is considerable larger than NN and NNN one can be understood by considering the contribution of direct-exchange interaction. For NN and NNN cases, the Fe-O-Fe angle of 90 ° indicates that the superexchange coupling favors FM, while the direct exchange favors AFM; see Fig. 2(d). Although superexchange dominates the NN and NNN interactions according to the Goodenough-Kanamori-Anderson (GKA) rules [40,41], the competition between these two effects makes the values of $J_1$ and $J_2$ rather small. For the NNN case, as shown in Fig. 2(e), the Fe-O-Fe angle of 180 ° suggests that superexchange coupling favors AFM, while direct exchange can be neglected due to the quite large Fe-Fe distance. As a consequence, $J_3$ is significantly larger than $J_1$ and $J_2$. Such phenomena are also observed in other 2D magnetic materials [41]. Based on these results, we can easily understand why single-layer $FeO_2H$ favors AFM-1 order.

Different from magnetism where local structure symmetry plays an important role, ferroelasticity relates to whole structure symmetry. A necessary condition for realizing ferroelasticity is the existence of two or more equally stable orientation variants, which can be switched from one to another in the presence of external stress. Such orientation variants normally originate from the structural phase transition that lowers the symmetry of a prototype phase. As we mentioned above, SL $FeO_2H$ belongs to space group $Pmn2_1$. This space group can be achieved by reducing the symmetry of space group $Abm_2$. The transformation from space group $Abm_2$ to space group $Pmn2_1$ could occur along both the $x$ and $y$ directions, forming two different orientations that are perpendicular to each other. In light of these, the appearance of ferroelastic order in SL $FeO_2H$ is highly expected.

Figure 3(a) shows the two ferroelastic ground states of SL $FeO_2H$, $F$ and $F'$. In initial variant $F$, the shorter lattice lies along the $b$ axis. By applying uniaxial tensile strain along the $b$ axis, the shorter lattice switches to the $a$ axis, giving rise to final invariant $F'$, where the lattice constants are $a'=|b|$ and $b'=|a|$. It should be noted that imposing uniaxial tensile strain on 2D materials is well established in previous experimental works [42–45]. Obviously, as shown in Fig. 3(a), final invariant $F'$ is similar to initial variant $F$ with a 90 ° rotation. Inverse transformation between final invariant $F'$ and initial variant $F$ can also be obtained when imposing uniaxial tensile on final invariant F′ along the $a$ axis. The displayed configuration $P$ in Fig. 3(a) with space group $Abm_2$ is supposed to be the paraelastic state of SL $FeO_2H$, with lattice constants $a'=b'=3.66$ Å. Such paraelastic state would undergo a spontaneous structural transformation to the ground states $F$ and $F'$.

To provide a better physical picture of the ferroelastic behaviors in SL $FeO_2H$, we further investigate the transformation pathway from initial invariant $F$ to final invariant $F'$ using the nudged elastic band (NEB) method. Figure 3(b) shows the minimum energy pathway of ferroelastic switching as a function of step number within NEB. According to the symmetry, the energy profile from $F$ to $P$ is identical to that from $F'$ to $P$. As shown in Fig. 3(b), the magnetic ground state is always AFM-1 during the ferroelastic switching process. The energy barrier for ferroelastic switching in SL $FeO_2H$ is estimated to be 54 meV/atom, which is dramatically smaller than that of phosphorene (0.20 eV/atom) [31], borophane (0.10 eV/atom)

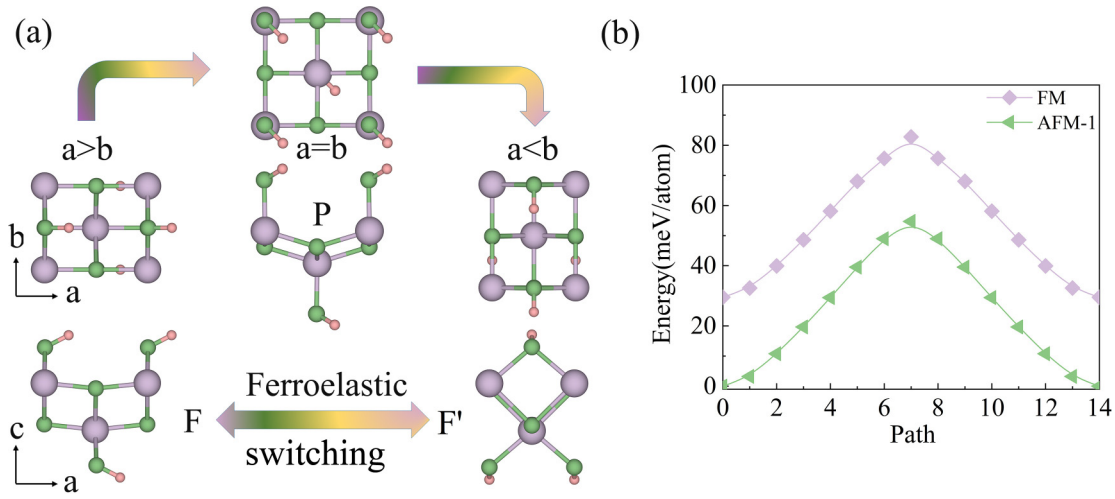


FIG. 3. Ferroelasticity of SL $FeO_2H$. (a) Schematic diagram of ferroelastic switching for SL $FeO_2H$. (b) Minimum energy pathway of ferroelastic switching as a function of step number within NEB for SL $FeO_2H$.

[46], $BP_5$ (0.32 eV/atom) [47], $\alpha$-MPI (0.13 eV/atom) [26], VSSe (0.23 eV/atom) [29], and GaTeCl (0.16 eV/atom) [48], and comparable to that of $1T'$-$WTe_2$ (73.3 meV/atom) [49]. Such a low barrier renders the high possibility of fast ferroelastic switching in SL $FeO_2H$ upon applying external stress. Besides the energy barrier, ferroelastic performance also depends on reversible ferroelastic strain, which controls the signal intensity and is defined as $|a/b-1| \times 100\%$. The obtained reversible ferroelastic strain for SL $FeO_2H$ is 23.5%, which is comparable with the values for $1S'$-MSSe (4.7%) [25], GeS (17.8%) [31], InOCl (17.7%) [50], $Nb_2GeTe_4$ (22.1%), and $Nb_2SiTe_4$ (24.4%) [51], suggesting a strong switching signal in SL $FeO_2H$. We therefore demonstrate the promising intrinsic ferroelastics in SL $FeO_2H$. It should be noted that, currently, the "Curie temperature" for ferroelastic behaviors can only be obtained in experiment and it is still challenging to estimate it theoretically. Of course the temperature will influence the ferroelastic properties, which is not discussed here.

Concerning space group $Pmn2_1$, it has one mirror symmetry only ($M_y : y \rightarrow -y$). The absence of mirror symmetry $M_x$ for SL $FeO_2H$ is attributed to the fact that the O-H bond deviates from the $c$ axis by $\theta_{max} = 60.5°$; see Fig. 1. Such deviation is very likely to induce spontaneous polarization in SL $FeO_2H$, and in turn yield ferroelectricity as long as the polarization is switchable. To confirm this speculation, we calculate the total polarization ($P_s$) of SL $FeO_2H$ employing the modern theory of polarization based on the Berry phase approach [52,53]. The intermediate state, where the O-H bond is aligned parallel along the $c$ axis, is taken as the paraelectric state (PE). The final ferroelectric state is obtained by swirling the angle between the O-H bond and the $c$ axis from $\theta_{max}$ to $-\theta_{max}$. We choose a structure deformation path between two FE states with the opposite spontaneous polarization and through a centrosymmetric reference structure to evaluate the spontaneous polarization as shown in Fig. 4(a). As shown in Fig. 4(a), SL $FeO_2H$ exhibits a spontaneous polarization $P_s$ of $0.68 \times 10^{-10}\,C\,m^{-1}$ along the $a$ axis. This value is comparable with that of SL As ($0.46 \times 10^{-10}\,C\,m^{-1}$) [54], $(CrBr_3)_2Li$ ($0.92 \times 10^{-10}\,C\,m^{-1}$), [27] and SnSe ($1.51 \times 10^{-10}\,C\,m^{-1}$) [55], and significantly larger than that of diisopropylammonium bromide ($1.5 \times 10^{-12}\,C\,m^{-1}$) [56] and $Hf_2VC_2F_2$ ($1.95 \times 10^{-12}\,C\,m^{-1}$) [57].

To further inspect the ferroelectricity, we study the ferroelectric switching process using the NEB method. The energy profiles of ferroelectric switching as a function step number are plotted in Fig. 4(b). The switching barrier $E_b$ for SL $FeO_2H$ is estimated to be 0.457 eV/unit cell, which is higher than that of $BP_5$ (0.41 eV/unit cell) [47], but much smaller than that of GaTeCl (0.754 eV/unit cell) [48]. Such moderate barrier enables the feasibility of ferroelectric switching in SL $FeO_2H$. As shown in Fig. S4 in the Supplemental Material [33], the magnetic ground state is always AFM-1 during the ferroelectric switching process.

The ferroelectricity in SL $FeO_2H$ can also be described by Landau theory [57,58]. The potential energy expressed in Landau-Ginzburg type expansion is given by Bruce [59],

$$E = \sum_i \frac{A}{2}(P_i^2) + \frac{B}{4}(P_i^4) + \frac{C}{6}(P_i^6) + \frac{D}{2}\sum_{\langle i,j\rangle}(P_i - P_j)^2,$$

which can be considered as the Taylor series of local structural distortions with a certain polarization defined at each cell $P_i$. The first three terms relate to energy contribution from local modes up to sixth order, which are viewed as the Landau energy part, while the last term is associated with interaction between the nearest local modes and can be given by mean-field theory within nearest neighbor approximation. The fitted energy versus polarization is shown in Fig. S5 [33], from which we can see a typical anharmonic double-well energy curve, again confirming the ferroelectricity in SL $FeO_2H$. It should be noted that the existence of ferroelectricity does not guarantee its stability with temperature. Spontaneous polarization would be suppressed when the temperature is above Curie temperature $T_C$. To this end, we investigate the Curie temperature $T_C$ for ferroelectricity of SL $FeO_2H$. By performing the MD simulations [60], the Curie temperature of SL $FeO_2H$ is estimated to be 260 K [Fig. 4(c)], suggesting its practical applications in 2D memory devices.

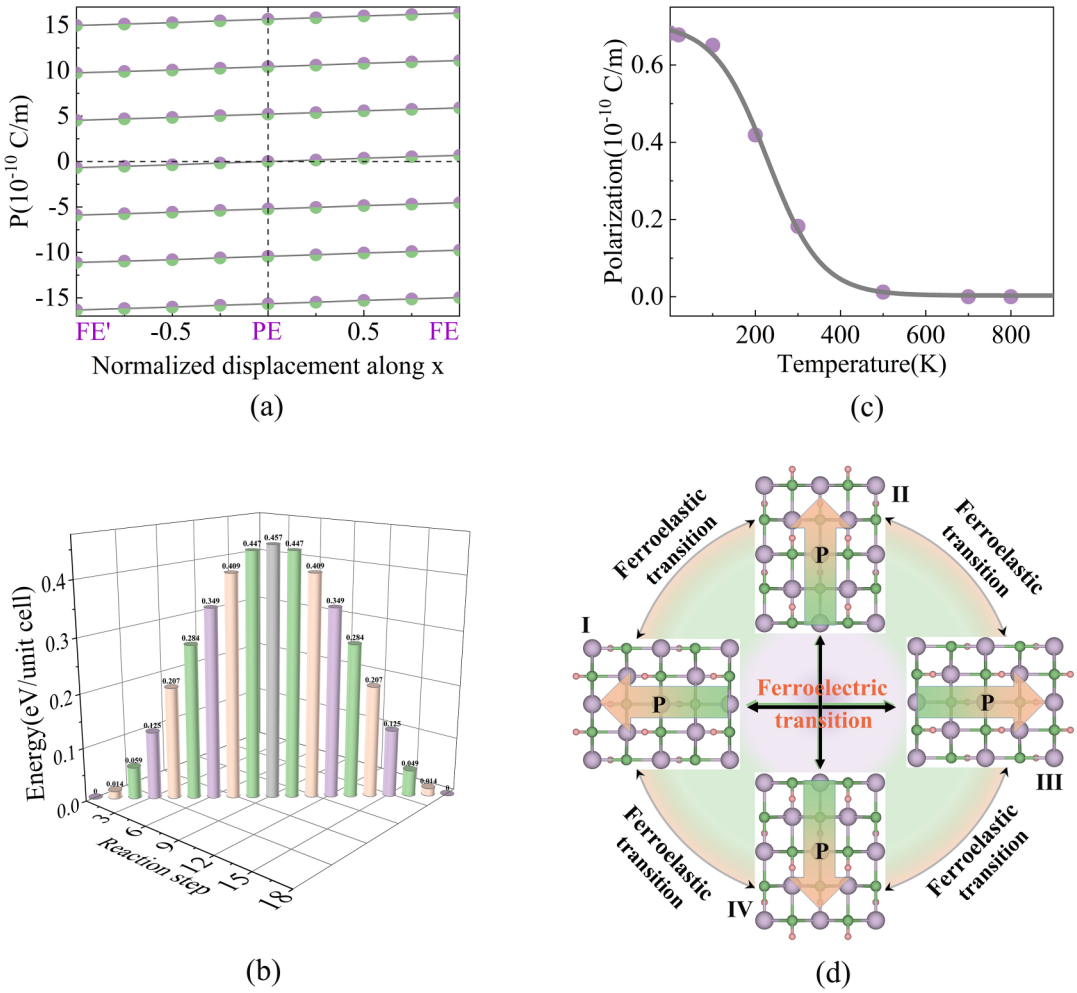


FIG. 4. Ferroelectricity of SL $FeO_2H$. (a) Total polarization as a function of normalized displacement for SL $FeO_2H$. The difference between those vertically shifted curves is known as the polarization quantum. (b) Energy profile of ferroelectric switching as a function of step number within NEB for SL $FeO_2H$. (c) Polarization as a function of temperature for SL $FeO_2H$ obtained from MD simulations. (d) Schematic diagram of the manipulation of the ferroelasticity orders by ferroelastic in SL $FeO_2H$. Fat arrows in (d) denote the directions of spontaneous polarization.

## III. DISCUSSION

From the above, we reveal that SL $FeO_2H$ is an intrinsically 2D triferroic semiconductor. These three ferroic orders could independently encode information in a single bit, meeting the long pursuit of multifunctional and high-density devices. Concerning the use of ferroelasticity to encode information, each ferroelastic phase corresponds to one information state [61]. The ferroelastic phase of SL $FeO_2H$ has two invariants with different spontaneous strain. Such difference in spontaneous strain renders external stress to couple energetically with the strain state of the system and drive orientation switch, which is analogous to the switching of spontaneous polarization by external electric field in a ferroelectric material [49]. It is also a major experimental undertaking to measure ferroelastic hysteresis [62]. We wish to point out that such coexistence of ferroic orders can also lead to fascinating physics and applications. For example, it is possible to realize the precise direction control of ferroelectric polarization $P_s$ in SL $FeO_2H$ through ferroelastic switching. As illustrated in Fig. 4(d), the lattice structure of SL $FeO_2H$ would experience a 90° rotation under the ferroelastic switching, subsequently causing a 90° rotation of polarization $P_s$. According to the symmetry, the direction of polarization $P_s$ in SL $FeO_2H$ is switchable among the $x$, $y$, $-x$, and $-y$ directions through 90° ferroelastic transition. Meanwhile, the ferroelastic switching can also be induced upon employing a higher-order electric field effect, which has been demonstrated in previous works [63,64]. Based on this fact, the electrically reading and mechanically writing four-state memory devices are being developed. The four-state information is stored by the polarization $P_s$ pointing to four directions (i.e., $x$, $y$, $-x$, and $-y$) that can be controlled by ferroelectric and ferroelastic transitions. Meanwhile, as the two ferroelastic states relate to the ferroelectric polarization $P_s$ pointing to $x/-x$ and $y/-y$ directions, respectively, these two ferroelastic states can be distinguished electrically. This is attractive as it exploits the best aspects of ferroelectric and ferroelastic data storages. In addition, as the easy axis of antiferromagnetism is along the $y$ axis, it would experience a 90° rotation under the ferroelastic switching, thus also achieving the precise direction control of the easy axis of antiferromagnetism in SL

$FeO_2H$ through ferroelastic switching. It is known that the possible atom vacancies can result in magnetization [65,66]. Therefore, the magnetic ground state and exchange interaction might be affected by the possible atom vacancies in SL $FeO_2H$.

Another interesting phenomenon in SL $FeO_2H$ we wish to address is the piezoelectric effect. In light of its symmetry, the unique piezoelectric coefficients for SL $FeO_2H$ are $e_{11}$ and $e_{12}$ are calculated. As listed in Table S4 [33], the value of $e_{11}$ is calculated to be $4.17 \times 10^{-10}$ C/m, which is much larger than that measured for SL $MoS_2$ [67], while for $e_{12}$, the value is estimated to be $-0.73 \times 10^{-10}$ C/m. According to the expressions $d_{11} = (e_{11}C_{22} - e_{12}C_{12}/C_{11}C_{22} - C_{12}^2)$ and $d_{12} = (e_{12}C_{11} - e_{11}C_{12}/C_{11}C_{22} - C_{12}^2)$, the piezoelectric coefficients $d_{11}$ and $d_{12}$ are found to be 2.39 and $-1.58$ pm/V, respectively. These values are larger than those of *h*-BN (0.60 pm/V) [68], and comparable to the values of SL $MoS_2$ (3.37 pm/V) [67]. Such in-plane piezoelectric effect in SL $FeO_2H$ would make it also potentially applicable in sensors and energy conversion devices.

Finally, we explore the experimental fabrication and stability of SL $FeO_2H$. Bulk $FeO_2H$ has been known since 1978 [69]. Figure S7 shows the crystal structure of bulk $FeO_2H$ [33]. It crystallizes in the space group $Cmc2_1$, showing a layered structure with two slabs in one unit cell. The optimized lattice parameters are found to be $a = 3.85$ Å, $b = 3.06$ Å, and $c = 11.91$ Å, which agrees well with those of the experiments (i.e., $a = 3.87$ Å, $b = 3.07$ Å, $c = 12.52$ Å) [70]. To fabricate SL $FeO_2H$ from layered bulks, mechanical cleavage and liquid exfoliation are feasible approaches. Our calculated cleavage energy of SL $FeO_2H$, $\sim$1.13 J/m$^2$, is similar to those of $Ca_2N$ (1.08 J/m$^2$) [71], $GeP_3$ (1.14 J/m$^2$) [72], and $InP_3$ (1.32 J/m$^2$) [73], which indicates that the cleavage from the layered $FeO_2H$ is accessible. To confirm the stability of SL $FeO_2H$, we investigate its phonon dispersions. As displayed in Fig. S7 [33], no imaginary phonon mode can be observed, demonstrating that SL $FeO_2H$ is dynamically stable. We also perform *Ab initio* molecular dynamics (AIMD) simulations to evaluate its thermal stability. The structure of SL $FeO_2H$ remains intact and the free energy fluctuates slightly during annealing within 6 ps (see Fig. S8) [33], indicating its thermal stability. Furthermore, we estimate its mechanical stability. The elastic constants of SL $FeO_2H$ are calculated to be $C_{11} = 162.76$ N/m, $C_{22} = 104.67$ N/m, $C_{12} = 41.06$ N/m, and $C_{44} = 18.24$ N/m. These values obey the mechanical stability criteria for a tetragonal monolayer: $C_{11}C_{22}{C_{12}}^2 > 0$ and $C_{66} > 0$ [74]. The stability analysis ensures that the triferroics predicted in SL $FeO_2H$ exhibits superior experimental feasibility.

In summary, using first-principles calculations, we reveal that SL $FeO_2H$ harbors antiferromagnetic, ferroelastic, and ferroelectric orders simultaneously, being an intrinsically 2D triferroic semiconductor. The physical origins of such triferroics are discussed in detail. We also show that such system can demonstrate many fascinating physics and applications, i.e., the directional control of ferroelectric polarization by ferroelastic switching and the in-plane piezoelectric effect. Moreover, SL $FeO_2H$ exhibits superior experimental feasibility as well as great stabilities. Our findings unveil the existence of triferroicity in 2D lattice and offer an ideal platform for studying 2D triferroics.

## IV. METHODS

### A. First-principles calculations

First-principles calculations are performed within the density functional theory as implemented in the Vienna *ab initio* simulation package [75,76]. The electron exchange correlation is described by the generalized gradient approximation (GGA) in the form of Perdew-Burke-Ernzerhof (PBE) [77]. The electron-ion interaction is treated by the projected augmented wave (PAW) method [78]. The PBE + $U$ method with $U = 5.0$ eV for the $d$ electrons is used to take strong correlation effects into account. Different $U$ values are tested, and the main conclusions are not affected (for more detail, please see Figs. S9 and S10 and Table S3 in the Supplemental Material [33]). Cutoff energy is set to be 450 eV. The vacuum space is set as 20 Å. The convergence criteria for energy and force are set to $1 \times 10^{-5}$ eV and 0.02 eV Å$^{-1}$, respectively. The Brillouin zone is sampled using the Monkhorst-Pack scheme [79]: $9 \times 9 \times 1$ for structural optimization and $11 \times 11 \times 1$ for self-consistent calculations. The lattice parameters are optimized in the NM, FM, and AFM-1 configurations, which show negligible difference. The HSE06 functional is adopted for accurately calculating band structures [80]. The phonon spectra are calculated based on density functional perturbation theory using the PHONOPY program [81]. AIMD simulations were performed with a $3 \times 3 \times 1$ supercell for 6 ps with a time step of 1 fs using a *NVT* ensemble. In order to obtain the Curie temperature from the MD simulations, the initial configuration in the supercell in the MD simulations is annealed at different temperatures. In this approach, the average polarization can be tracked in the simulations, without any fitting parameters. Lastly, we adopt the Sigmoid form with $P(T) = a - a/(1 + e^{(b-T_c)})$, where $a$ and $b$ are constants, to fit the results from molecular dynamic simulations. The ferroelectric polarization is evaluated using the Berry phase method [53]. The dispersion interaction was accounted for by using Grimme's DFT-D3 method [82].

The datasets that support the findings of this study are available from the corresponding author on reasonable request.

## ACKNOWLEDGMENTS

This work is supported by the National Natural Science Foundation of China (Grants No. 11804190 and No. 12074217), Shandong Provincial Natural Science Foundation (Grants No. ZR2019QA011 and No. ZR2019MEM013), Shandong Provincial Key Research and Development Program (Major Scientific and Technological Innovation Project No. 2019JZZY010302), Shandong Provincial Key Research and Development Program (Program No. 2019RKE27004), Shandong Provincial Science Foundation for Excellent Young Scholars (Grant No. ZR2020YQ04), Qilu Young Scholar Program of Shandong University, and Taishan Scholar Program of Shandong Province.

The authors declare no competing financial interest.

[1] A. Von Hippel, R. G. Breckenridge, F. G. Chesley, and L. Tisza, Ind. Eng. Chem. **38**, 1097 (1946).
[2] B. T. Matthias, Science **113**, 591 (1951).
[3] K. Aizu, J. Phys. Soc. Jpn. **27**, 387 (1969).
[4] V. K. Wadhawan, *Introduction to Ferroic Materials* (Gordon and Breach, New York, 2000).
[5] W. Eerenstein, N. D. Mathur, and J. F. Scott, Nature **442**, 759 (2006).
[6] J.-Y. Chauleau, T. Chirac, S. Fusil, V. Garcia, W. Akhtar, J. Tranchida, P. Thibaudeau, I. Gross, C. Blouzon, A. Finco, M. Bibes, B. Dkhil, D. D. Khalyavin, P. Manuel, V. Jacques, N. Jaouen, and M. Viret, Nat. Mater. **19**, 386 (2020).
[7] P. Lunkenheimer, J. Müller, S. Krohns, F. Schrettle, A. Loidl, B. Hartmann, R. Rommel, M. Souza, C. Hotta, J. A. Schlueter, and M. Lang, Nat. Mater. **11**, 755 (2012).
[8] Y. S. Oh, S. Artyukhin, J. J. Yang, V. Zapf, J. W. Kim, D. Vanderbilt, and S. W Cheong, Nat. Commun. **5**, 3201 (2014).
[9] N. A. Spaldin and M. Fiebig, Science **309**, 391 (2005).
[10] N. Hur, S. Park, P. A. Sharma, J. S. Ahn, S. Guha, and S-W. Cheong, Nature **429**, 392 (2004).
[11] D. D. Sante, A. Stroppa, P. Jain, and S. Picozzi, J. Am. Chem. Soc. **135**, 18126 (2013).
[12] C. Xu, L. B. Wang, Z. B. Liu, L. Chen, J. K. Guo, N. Kang, X. L. Ma, H. M. Cheng, and W. C. Ren, Nat. Mater. **14**, 1135 (2015).
[13] J. Bekaert, M. Petrov, A. Aperis, P. M. Oppeneer, and M. V. Milošević, Phys. Rev. Lett. **123**, 077001 (2019).
[14] R. Yu, W. Zhang, H. J. Zhang, S. C. Zhang, X. Dai, and Z. Fang, Science **329**, 61 (2010).
[15] C. L. Kane and E. J. Mele, Phys. Rev. Lett. **95**, 226801 (2005).
[16] Y. D. Ma, L. Z. Kou, Y. Dai, and T. Heine, Phys. Rev. B **94**, 201104(R) (2016).
[17] D. Sarkar, X. J. Xie, W. Liu, W. Cao, J. H. Kang, Y. J. Gong, S. Kraemer, P. M. Ajayan, and K. Banerjee, Nature **526**, 91 (2015).
[18] L. K. Li, Y. J. Yu, G. J. Ye, Q. Q. Ge, X. D. Ou, H. Wu, D. L. Feng, X. H. Chen, and Y. B. Zhang, Nat. Nanotechnol. **9**, 372 (2014).
[19] M. H. Wu, S. Dong, K. L. Yao, J. M. Liu, and X. C. Zeng, Nano Lett. **16**, 7309 (2016).
[20] W. Luo and H. J. Xiang, Angew. Chem. **128**, 8717 (2016).
[21] K. Chang, J. W. Liu, H. C. Lin, N. Wang, K. Zhao, A. M. Zhang, F. Jin, Y. Zhong, X. P. Hu, W. H. Duan, Q. M. Zhang, L. Fu, Q. K. Xue, X. Chen, and S. H. Ji, Science **353**, 274 (2016).
[22] C. Gong, L. Li, Z. L. Li, H. W. Ji, Y. Xia, A. Stern, T. Cao, W. Bao, C. Z. Wang, Y. Wang, Z. Q. Qiu, R. J. Cava, S. G. Louie, J. Xia, and X. Zhang, Nature **546**, 265 (2017).
[23] B. Huang, G. Clark, E. Navarro-Moratalla, D. R. Klein, R. Cheng, K. L. Seyler, D. Zhong, E. Schmidgall, M. A. McGuire, D. H. Cobden, W. Yao, D. Xiao, P. Jarillo-Herrero, and X. D. Xu, Nature **546**, 270 (2017).
[24] N. H. Miao, B. Xu, L. G. Zhu, J. Zhou, and Z. M. Sun, J. Am. Chem. Soc. **140**, 2417 (2018).
[25] Y. D. Ma, L. Z. Kou, B. B. Huang, Y. Dai, and T. Heine, Phys. Rev. B **98**, 085420 (2018).
[26] T. Zhang, Y. D. Ma, L. Yu, B. B. Huang, and Ying Dai, Mater. Horiz. **6**, 1930 (2019).
[27] C. X. Huang, Y. P. Du, H. P. Wu, H. J. Xiang, K. M. Deng, and E. J. Kan, Phys. Rev. Lett. **120**, 147601 (2018).
[28] L. Yang, M. H. Wu, and K. L. Yao, Nanotechnology **29**, 215703 (2018).
[29] C. M. Zhang, Y. H. Nie, S. Sanvito, and A. J. Du, Nano Lett. **19**, 1366 (2019).
[30] X. Tang and L. Z. Kou, J. Phys. Chem. Lett. **10**, 6634 (2019).
[31] M. H. Wu and X. C. Zeng, Nano Lett. **16**, 3236 (2016).
[32] H. Wang and X. F. Qian, 2D Mater. **4**, 015042 (2017).
[33] See Supplemental Material at http://link.aps.org/supplemental/10.1103/PhysRevB.103.144101 for more computational details and results about the effect of Hubbard $U$ and SOC, magnetic configuration, magnetocrystalline anisotropy energy, parameter of the exchange coupling, energy profiles of ferroelectric transition for SL $FeO_2H$ under different magnetic configurations, double-well potential, crystal structure of bulk $FeO_2H$, AIMD simulations, electronic structures, atomic coordinates and Wyckoff positions, and piezoelectric coefficients.
[34] L. Hu, X. J. Wu, and J. L. Yang, Nanoscale **8**, 12939 (2016).
[35] Y. L. Jiao, W. K. Wu, F. X. Ma, Z. M. Yu, Y. H. Lu, X. L. Sheng, Y. W. Zhang, and S. A. Yang, Nanoscale **11**, 16508 (2019).
[36] H. L. Zhang, P. R. C. Kent, and R. G. Hennig, Phys. Rev. B **93**, 134407 (2016).
[37] Y. M. Fang, S. Q. Wu, Z. Z. Zhu, and G. Y. Guo, Phys. Rev. B **98**, 125416 (2018).
[38] G. Y. Guo, W. Temmerman, and H. Ebert, J. Phys.: Condens. Matter **3**, 8205 (1991).
[39] J. M. Kosterlitz, J. Phys. C: Solid State Phys. **7**, 1046 (1974).
[40] J. Kanamori, J. Phys. Chem. Solids **10**, 87 (1959).
[41] W. Geertsma and D. Khomskii, Phys. Rev. B **54**, 3011 (1996).
[42] D. C. Zhang, A. Rahman, W. Qin, X. Li, P. Cui, Z. Zhang, and Z. Zhang, Phys. Rev. B **101**, 205119 (2020).
[43] Y. C. Du, J. Maassen, W. R. Wu, Z. Luo, X. F. Xu, and P. D. Ye, Nano Lett. **16**, 6701 (2016).
[44] K. L. He, C. Poole, K. F. Mak, and J. Shan, Nano Lett. **13**, 2931 (2013).
[45] A. McCreary, R. Ghosh, M. Amani, J. Wang, K. N. Duerloo, A. Sharma, K. Jarvis, E. J. Reed, A. M. Dongare, S. K. Banerjee, M. Terrones, R. R. Namburu, and M. Dubey, ACS Nano **10**, 3186 (2016).
[46] L. Z. Kou, Y. D. Ma, C. Tang, Z. Sun, A. J. Du, and C. F. Chen, Nano Lett. **16**, 7910 (2016).
[47] H. D. Wang, X. X. Li, J. Y. Sun, Z. Liu, and J. L. Yang, 2D Mater. **4**, 045020 (2017).
[48] S. H. Zhang and B. G. Liu, Nanoscale **10**, 5990 (2018).
[49] W. B. Li and J. Li, Nat. Commun. **7**, 10843 (2016).
[50] X. L. Xu, Y. D. Ma, B. B. Huang, and Y. Dai, Phys. Chem. Chem. Phys. **21**, 7440 (2019).
[51] T. Zhang, Y. D. Ma, X. L. Xu, C. A. Lei, B. B. Huang, and Y. Dai, J. Phys. Chem. Lett. **11**, 497 (2020).
[52] R. Resta, Rev. Mod. Phys. **66**, 899 (1994).
[53] R. D. King-Smith and D. Vanderbilt, Phys. Rev. B **47**, 1651 (1993).
[54] C. C. Xiao, F. Wang, S. A. Yang, Y. H. Lu, Y. P. Feng, and S. B. Zhang, Adv. Funct. Mater. **28**, 1707383 (2018).
[55] R. X. Fei, W. Kang, and L. Yang, Phys. Rev. Lett. **117**, 097601 (2016).
[56] L. Ma, Y. L. Jia, S. Ducharme, J. L. Wang, and X. C. Zeng, J. Am. Chem. Soc. **141**, 1452 (2019).
[57] J. Zhang, L. Lin, Y. Zhang, M. Wu, B. I. Yakobson, and S. Dong, J. Am. Chem. Soc. **140**, 9768 (2018).

[58] H. E. Stanley, *Introduction to Phase Transitions and Critical Phenomena* (Clarendon Press, Oxford, 1971).
[59] A. D. Bruce, Adv. Phys. **29**, 111 (1980).
[60] R. N. Barnett and U. Landman, Phys. Rev. B **48**, 2081 (1993).
[61] E. K. H. Salje, *Phase Transitions in Ferroelastic and Coelastic Crystals* (Cambridge University Press, Cambridge, 1990).
[62] E. K. H. Salje, Annu. Rev. Mater. Res. **42**, 265 (2012).
[63] J. Zhou, H. Xu, Y. Li, R. Jaramillo, and J. Li, Nano Lett. **18**, 7794 (2018).
[64] Y. M. Pan and J. Zhou, Phys. Rev. Appl. **14**, 014024 (2020).
[65] H. Pan, J. B. Yi, L. Shen, R. Q. Wu, J. H. Yang, J. Y. Lin, Y. P. Feng, J. Ding, L. H. Van, and J. H. Yin, Phys. Rev. Lett. **99**, 127201 (2007).
[66] X. J. Wang, Y. L. Song, L. L. Tao, J. F. Feng, Y. Sui, J. K. Tang, B. Song, Y. Wang, Y. Wang, Y. Zhang, and X. F. Han, Appl. Phys. Lett. **105**, 262402 (2014).
[67] H. Y. Zhu, Y. Wang, J. Xiao, M. Liu, S. M. Xiong, Z. J. Wong, Z. L. Ye, Y. Ye, X. B. Yin, and X. Zhang, Nat. Nanotechnol. **10**, 151 (2015).
[68] K.-A. N. Duerloo, M. T. Ong, and E. J. Reed, J. Phys. Chem. Lett. **3**, 2871 (2012).
[69] H. Christensen and A. N. Christensen, Acta Chem. Scand. **32a**, 87 (1978).
[70] Y. Song, Y. Cao, J. Wang, Y.-N. Zhou, F. Fang, Y. S. Li, S.-P. Gao, Q.-F. Gu, L. F. Hu, and D. L. Sun, ACS Appl. Mater. Interfaces **8**, 21334 (2016).
[71] S. T. Zhao, Z. Y. Li, and J. L. Yang, J. Am. Chem. Soc. **136**, 13313 (2014).
[72] Y. Jing, Y. D. Ma, Y. F. Li, and T. Heine, Nano Lett. **17**, 1833 (2017).
[73] N. H. Miao, B. Xu, N. C. Bristowe, J. Zhou, and Z. M. Sun, J. Am. Chem. Soc. **139**, 11125 (2017).
[74] J. Wang, S. Yip, S. R. Phillpot, and D. Wolf, Phys. Rev. Lett. **71**, 4182 (1993).
[75] G. Kresse and J. Furthmuller, Phys. Rev. B **54**, 11169 (1996).
[76] G. Kresse and J. Furthmuller, Comput. Mater. Sci. **6**, 15 (1996).
[77] J. P. Perdew, K. Burke, and M. Ernzerhof, Phys. Rev. Lett. **77**, 3865 (1996).
[78] G. Kresse and D. Joubert, Phys. Rev. B **59**, 1758 (1999).
[79] H. J. Monkhorst and J. D. Pack, Phys. Rev. B **13**, 5188 (1976).
[80] J. Heyd and G. E. Scuseria, J. Chem. Phys. **118**, 8207 (2003).
[81] X. Gonze and C. Lee, Phys. Rev. B **55**, 10355 (1997).
[82] S. Grimme, S. Ehrlich, and L. Goerigk, J. Comput. Chem. **32**, 1456 (2011).